Eur. Phys. J. B **60**, 483–491 (2007)
DOI: 10.1140/epjb/e2008-00004-6

THE EUROPEAN PHYSICAL JOURNAL B

Wavelet transform modulus maxima based fractal correlation analysis

D.C. Lin[a] and A. Sharif

Department of Mechanical and Industrial Eng., Ryerson University, Toronto, ON, Canada

Received 15 February 2007 / Received in final form 25 October 2007
Published online 16 January 2008 –

Abstract. The wavelet transform modulus maxima (WTMM) used in the singularity analysis of one fractal function is extended to study the fractal correlation of two multifractal functions. The technique is developed in the framework of joint partition function analysis (JPFA) proposed by Meneveau et al. [C. Meneveau, K.R. Sreenivasan, Phys. Rev. A **41**, 894 (1990)] and is shown to be equally effective. In addition, we show that another leading approach developed for the same purpose, namely, relative multifractal analysis, can be considered as a special case of JPFA at a particular parameter setting.

PACS. 05.45.Df Fractals – 05.45.Tp Time series analysis

1 Introduction

Fluctuations in many natural and artificial phenomena are found to exhibit fractal characteristics. In applications, this has been characterized by the so-called singularity spectrum of some numerical or experimental data [1–9]. To understand the fractal dynamics underlying phenomenology, multiple data capturing different aspects of the phenomenon of interest are sometimes used together in the analysis. For example, velocity and temperature fluctuations are used to analyze the momentum and energy aspects of the multifractal hydrodynamic turbulence [1], blood pressure and heart rate fluctuations to analyze the cardiovascular aspect of the $1/f$-like power spectrum of the heart rate variability in humans [10], and packet size and arrival time to analyze the congestion and connectivity aspects of the multifractal network traffic [11]. Fractal analysis on multiple data provides an unique opportunity to relate different manifestations of the fractality of the phenomenon. In particular, one would suspect some degree of *fractal correlation* in the data if the fractal generating mechanisms associated with the data source are coupled together.

Essential to the notion of fractal correlation is the distinguishability of singularity spectra. There are fundamental and practical issues related to the subject. For example, consider a standard N_p-adic multinomial process on an interval. It is a multiplicative cascade constructed by repeatedly dividing the interval into equal N_p segments and assigning (probability) weights $p_i, i = 1, \ldots, N_p$, from one generation to the next. Continuing this procedure *ad infinitum* leads to a limiting process with no density (almost surely) and intermittent spiking pattern. Its singularity spectrum $f_\pi(\alpha)$ may be estimated by the Legendre transform of $\tau_\pi(q) = -\log(\sum p_i^q)/\log(N_p)$:

$$f_\pi(\alpha) = q\alpha - \tau_\pi(q)$$

where $\alpha(q) = d\tau_\pi/dq$. Now, consider a different N_m-adic cascade ($N_m \neq N_p$) generated by weights $m_i, i = 1, \ldots, N_m$, and its singularity spectrum $f_\mu(\alpha)$. If $f_\pi(\alpha) = f_\mu(\alpha)$, one must have

$$\sum p_i^q = \left(\sum m_i^q\right)^{\log(N_p)/\log(N_m)}.$$

However, no $\{p_i\}$ and $\{m_i\}$ can be found to satisfy this equation for all q. Thus, singularity spectra can in theory be distinguished, at least for the important class of multinomial processes. For more in-depth treatments and examples, see the excellent book by Pesin [12].

In practice, a different issue can arise. That is, two singularity spectra may be close to each other within the limit of finite precision. Consider again the cascades from above. Let $\tau_\pi(-\infty) = \tau_\mu(-\infty)$, $\tau_\pi(+\infty) = \tau_\mu(+\infty)$ (so $\max(\{p_i\}) = \max(\{m_i\})^{\log(N_p)/\log(N_m)}$, $\min(\{p_i\}) = \min(\{m_i\})^{\log(N_p)/\log(N_m)}$). Then, $f_\pi(\alpha), f_\mu(\alpha)$ will agree at four important q values: $-\infty, +\infty, 0, 1$. With the rest of p_i and m_i chosen properly, they can be made almost indistinguishable (Fig. 1). This problem was addressed by Lévy-Léhel and Vojak who developed a much sharper mutual multifractal analysis to relate the singularity spectra to the generation of multinomial processes [13]. Riedi and Scheuring arrived at the similar relative multifractal analyses with further details on the numerical implementation [14]; see also [15,16]. For experimental data, Meneveau et al. introduced a joint partition function analysis (JPFA) based on the 1D version introduced by Hentschel and Procaccia [17] and Halsey et al. [18]. With

[a] e-mail: derlin@ryerson.ca

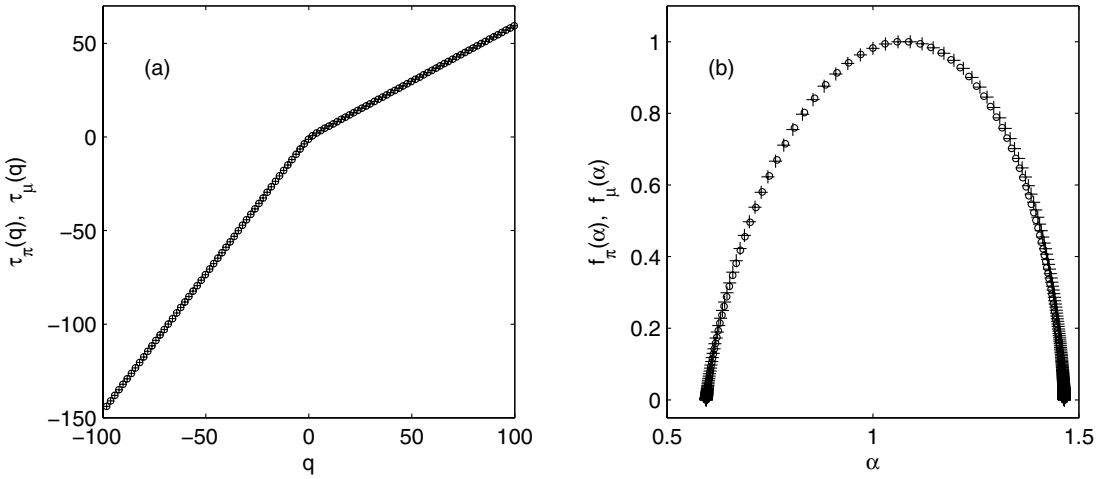

Fig. 1. Multifractal analyses of 3-adic π-cascade of weights 0.2, 0.28, 0.52 (symbol "o") and 5-adic μ-cascade of weights 0.09463, 0.1200, 0.1800, 0.2217, 0.3837 (symbol "+"). (a) $\tau_\pi(q)$ and $\tau_\mu(q)$; (b) $f_\pi(\alpha)$ and $f_\mu(\alpha)$.

essentially the same procedure of estimating the singularity spectrum, these authors characterized fractal correlation in the small scale kinetic energy transfer, heat concentration and vorticity of the turbulent flow [1]. They implied that multiple cascades of more than one variables are responsible for the fractal fluctuation in fluid turbulence; see also [19]. The JPFA has also been applied in diverse areas such as precision agriculture [20], soil property [21], and re-emerged in the general discussion of discrete scale invariance of the multinomial process [22].

In these past studies, JPFA as well as most singularity analyses were conducted on the assumption of one-dimensional multifractal measures and solved using the classical box counting procedure. Such applications can be limited in scope when, typically in the experimental study, the data is only a fractal function. For functions created by the integral of multinomial measure under C^∞ perturbation, Bacry et al. proved that the singularity analysis developed for the fractal measure is equally applicable by using the so-called wavelet transform modulus maxima (WTMM) method [2]. Later, the validity of WTMM was examined by Jaffard for any function [3]. Regarding WTMM, it was proved that (i) it can yield the upper bound estimate of the singularity spectrum for any function and (ii) it is exact for the so-called self-similar fractal function, as long as the so-called maxima lines are not too close to each others.

The purpose of this study is to introduce a joint WTMM method to carry out the JPFA of fractal correlation. While the term correlation is normally linked to the second order statistics, fractal correlation as estimated from the singularity spectra is a property of moment of all orders. Indeed, the primary object of the analysis is the Hausdorff dimension $f(\alpha_1, \alpha_2)$ of the support of observing Hölder exponents α_1 and α_2. It will be shown that $f(\alpha_1, \alpha_2)$ describes a two-dimensional surface that can be related to how fractal generating mechanisms are coupled to each other. In addition, it is also found that JPFA is a more general formulation in that the existing relative multifractal analysis developed for the similar purpose is related to JPFA at a particular parameter setting.

Our results are organized into four sections. In the next section, the background of WTMM is first summarized. The extension to the WTMM-based JPFA and its connection to the relative multifractal spectrum are then demonstrated. The test of the method using binomial cascades are presented in Section 3. Concluding remarks are given in Section 4.

2 WTMM–based fractal correlation analysis

2.1 WTMM singularity analysis

Singularity analysis is built on the notion of Hölder continuity of functions. Recall that a function $x(t)$ is Hölder continuous of exponent α' if there are $\alpha', \delta_0, C \in \mathbf{R}^+$, such that, for $\delta < \delta_0$,

$$|x(t_0 + \delta) - x(t_0)| \leq C|\delta|^{\alpha'}.$$

In the neighborhood of $x(t_0)$, there exists a supremum $\alpha(t_0)$ that (1) is valid for all $\alpha' \leq \alpha(t_0)$. The exponent $\alpha(t_0)$ is the Hölder exponent of $x(t)$ at t_0. Formally [2, 3], one can find an nth order polynomial $P_n(t)$ and $\alpha(t_0) \in [n, n+1)$ such that

$$|x(t_0 + \delta) - P_n(t_0)| \leq C|\delta|^{\alpha(t_0)}. \quad (1)$$

It is evident that the Hölder exponent characterizes the differentiability of the function and, thus, the ability of the function to fluctuate. For example, $\alpha = +\infty$ for C^∞ functions, $\alpha \in (n, n+1)$ for functions that are only n times differentiable and $\alpha < 1$ for functions that are non-differentiable. The $\alpha < 1$ case draws the most attention since it means the function can fluctuate in large amplitude over short time intervals and gives rise to the

so-called intermittent pattern witnessed in many physical systems. The Hölder exponent $\alpha(t)$ is also known as the singularity exponent.

The natural tool to analyze the singularity property is by the wavelet transform:

$$T_\psi[x](t,a) = \frac{1}{a}\int_{-\infty}^{\infty} \psi\left(\frac{t'-t}{a}\right) x(t')dt' \tag{2}$$

where $T_\psi[x](t,a)$ is the wavelet coefficient and $\psi(t)$ is the analyzing wavelet. Muzy et al. showed that the exponent $\alpha(t)$ can be estimated effectively using the supremum of $|T_\psi[x]|$ along the so-called maxima line formed by the local wavelet modulus maxima [2–5]. Denote the set of maxima lines at scale a by $\mathcal{L}(a) = \{l_1, l_2, \cdots, l_{N(a)}\}$. Bacry et al. proved [2]

$$Z(a;q) = \sum_{l_i \in \mathcal{L}(a)} C_i^q \sim a^{\tau(q)} \tag{3}$$

where $C_i = \sup_{(t,a)\in l_i} |T_\psi[x](t,a)|$ is the supremum of the modulus maxima of the maxima line l_i. For functions created by the integral of multinomial measures under C^∞ perturbations, it was shown that the Legendre transform of $\tau(q)$ yields the Hausdorff dimension of the support $\{t, \alpha(t) = \alpha\}$, $f(\alpha)$;

$$\tau(q) = \min_\alpha (q\alpha - f(\alpha)). \tag{4}$$

In the literature, $Z(a;q)$ is sometimes referred to as the partition function due to its analogy to the energy partition function in statistical mechanics.

2.2 WTMM-based JPFA of fractal correlation

Based on JPFA, the WTMM is generalized to study the fractal correlation in this section. We present the application of JPFA of two data sets. The extension to more data sets is conceptually similar.

Consider $x_1(t), x_2(t)$ and their respective sets of singularity exponent $\{\alpha_1\}, \{\alpha_2\}$. Let the maxima lines of $|T_\psi[x_k]|$ at scale a be denoted as $\mathcal{L}_k(a), k = 1, 2$. A natural extension of the existing WTMM analysis is to consider a joint partition function of the form:

$$Z(a;q_1,q_2) = \sum_j C_{1,r(j)}^{q_1} C_{2,s(j)}^{q_2} \tag{5}$$

where $C_{1,r}, C_{2,s}$ are the modulus maxima of the maxima lines $l_{1,r} \in \mathcal{L}_1, l_{2,s} \in \mathcal{L}_2$.

To realize (5), the maxima lines in $\mathcal{L}_k, k = 1, 2$ must be paired up properly (so the index j can run). As in most correlation analyses, the objective here is to characterize the property related to observing both singularity exponents α_1 and α_2. In terms of the WTMM analysis, such information should be contained in the modulus of the neighboring maxima lines. If the time coordinate of $l_{k,j}(a)$ is denoted by $t_{k,j}(a)$, this means the coefficients $C_{1,r}$, $C_{2,s}$ paired up in (5) can be determined by

$$|t_{1,r} - t_{2,s}| = \min_{r'}(|t_{1,r'} - t_{2,s}|) = \min_{s'}(|t_{1,r} - t_{2,s'}|). \tag{6}$$

Once (5) and (6) are established, similar procedure developed by Bacry et al. [2,4] can be extended to characterize the geometry associated with the observation of α_1 and α_2. In particular, based on $C_{k,\lambda} \sim a^{\alpha_k(\lambda)}$, $\lambda = r, s$, (5) can be given by

$$\begin{aligned} Z(a;q_1,q_2) &\sim \sum_j a^{q_1\alpha_1(r(j))+q_2\alpha_2(s(j))} \\ &= \int\int d\alpha_1 d\alpha_2 \mathcal{P}(\alpha_1,\alpha_2) a^{q_1\alpha_1+q_2\alpha_2} a^{-f(\alpha_1,\alpha_2)} \end{aligned} \tag{7}$$

where $\mathcal{P}(\alpha_1,\alpha_2)$ and $f(\alpha_1,\alpha_2)$ are the probability density function and Hausdorff dimension of the support of (α_1,α_2), respectively. Applying the standard argument of steepest descent in small a yields

$$Z(a;q_1,q_2) \sim a^{\tau(q_1,q_2)} \tag{8}$$

where

$$\tau(q_1,q_2) = \min_{\alpha_1,\alpha_2}(q_1\alpha_1 + q_2\alpha_2 - f(\alpha_1,\alpha_2)). \tag{9}$$

Hence, $\tau(q_1,q_2)$ and $f(\alpha_1,\alpha_2)$ are Legendre transform pair:

$$\begin{aligned} \alpha_1 = \partial\tau(q_1,q_2)/\partial q_1, \alpha_2 = \partial\tau(q_1,q_2)/\partial q_2, \\ f(\alpha_1,\alpha_2) = \alpha_1(q_1,q_2)q_1 + \alpha_2(q_1,q_2)q_2 - \tau(q_1,q_2) \end{aligned} \tag{10}$$

where

$$q_1 = \partial f/\partial\alpha_1, q_2 = \partial f/\partial\alpha_2. \tag{11}$$

Finally, from (9)–(11), the correlation coefficient between α_1, α_2 can be determined using $\tau(q_1,q_2)$:

$$\rho = \frac{\mathrm{cov}(\alpha_1,\alpha_2)}{\sigma_{\alpha_1}\sigma_{\alpha_2}} = -\left.\frac{\frac{\partial^2\tau}{\partial q_1\partial q_2}}{\sqrt{\left[\frac{\partial^2\tau}{\partial q_1^2}\frac{\partial^2\tau}{\partial q_2^2}\right]}}\right|_{q_1=q_2=0} \tag{12}$$

where cov denotes the covariance and σ_λ denotes the standard deviation of λ. This expression will be used in the next section to compare with the numerical result.

In the numerical experiment presented below, we did not directly apply (8)–(10) to estimate $\tau(q_1,q_2)$ and $f(\alpha_1,\alpha_2)$. Instead, we follow an alternative approach motivated by the canonical ensemble in statistical mechanics [6]. As shown in the Appendix A, this approach is able to circumvent certain numerical issue caused by the scale dependent prefactor in (8) [1,6,7].

2.3 JPFA and relative multifractal analysis

Relative multifractal analysis and similar ideas were developed to characterize fractal correlation between fractal measures. The main idea is to replace the use of Lebesgue measure in the traditional fractal analysis [13–16]. Specifically, consider the partition functions of multifractal measures π and μ

$$\sum_{A\in\mathcal{H}} \pi(A)^q \sim |A|^{\tau_\pi(q)}, \sum_{A'\in\mathcal{H}'} \mu(A')^q \sim |A'|^{\tau_\mu(q)} \tag{13}$$

where $\mathcal{H}, \mathcal{H}'$ denote generic partitions of the support and $|\cdot|$ denote the Lebesgue measure of the set. To examine the extent to which the singularity of π correlate with μ, the sets which scale as a power law will be characterized by using π. For example, the partition function of π is now written as

$$\sum \pi(A)^q \mu(A)^{-\mathbf{t}(q)} \sim O(|A|) \tag{14}$$

where the "big O" describes the order relationship $O(|A|) \to$ const. as $|A| \to 0$. Define $\tau_{\pi/\mu}(q) = \sup\{\mathbf{t}(q)\}$ for which (14) holds. The relative multifractal spectrum is obtained via the Legendre transform of $\tau_{\pi/\mu}$. It characterizes the support of the singular behaviour of the form $\pi \sim \mu^{\alpha_{\pi/\mu}(q)}$ where $\alpha_{\pi/\mu}(q) = d\tau_{\pi/\mu}(q)/dq$. The relative multifractal analysis can draw a much sharper distinction between π and μ. For example, $\tau_{\pi/\mu}(q)$ is nonlinear when $\pi \neq \mu$ and $\tau_{\pi/\mu}(q) = q - 1$ when $\pi = \mu$; see [14] for more details.

Comparison of (14) with (5) and (8) suggests $\tau_{\pi/\mu}$ can be obtained as the level set of $\tau(q_1, q_2) = 0$ where

$$q_2 = -\tau_{\pi/\mu}(q_1). \tag{15}$$

By switching the role of q_1, q_2, the singular behaviour of μ can be gauged by π in a similar way. With the same arguments, one arrives at $\tau_{\mu/\pi}(q_2)$ defined by the same level set $\tau(q_1, q_2) = 0$ where $q_1 = -\tau_{\mu/\pi}(q_2)$. It may be useful to point out that $\tau_{\pi/\mu}, \tau_{\mu/\pi}$ on the $q_1 \times q_2$ plane are nothing but mirror images of the level set $\{\tau(q_1, q_2) = 0\}$ about $q_2 = 0$ and $q_1 = 0$ axes, respectively.

3 Numerical experiments and results

3.1 Coupled random binomial cascades [1]

To test if the WTMM-based JPFA can reliably characterize fractal correlation, numerical experiments were conducted on the coupled random binomial cascades studied by Meneveau et al. [1]. For completeness, we shall introduce the coupled cascades and specific results relevant to the numerical tests.

The first cascade π, referred to as the π-cascade, is generated by weights p_0, p_1. Let $I_{r_1,\cdots,r_J}$ denote an interval segment generated in the Jth iteration where $r_i \in \{0, 1\}$ and $\sum r_i 2^{-i}$ is the based-2 coarse-grained representation of any $x \in I_{r_1,\cdots,r_J}$. By the multiplicative rule, $\pi(I_{r_1,\cdots,r_J}) = \prod_{j=1}^{J} p_{r_j}$. The second cascade μ, referred to as the μ-cascade, is generated by weights m_0, m_1 and $\mu(I_{s_1,\cdots,s_J}) = \prod_{j=1}^{J} m_{s_j}$, $s_i \in \{0, 1\}$ with the same addressing scheme.

To couple the cascades, a parameter g and a uniform random variable γ in [0,1] are used. Let I_L, I_R be the new segments created in the construction of the cascades. If $\gamma < g$, the weights assigned to I_L, I_R for the μ-cascade will depend on exactly how the weights of the π-cascade are assigned. In particular, if p_0 is assigned to I_L (I_R) of the π-cascade, m_0 will be assigned to I_L (I_R) of the μ-cascade and similarly for p_1 and m_1. If $\gamma \geq g$, the weight assignment for the cascades will be completely independent from each other. This way, the fractal generating mechanisms of the cascades are completely dependent of each other when $g = 1$ and independent of each other when $g = 0$.

For this example, the analytical $\tau(q, p)$ has a closed-form expression:

$$\tau(q_1, q_2) = -\log_2(2Y) \tag{16}$$

where

$$Y = \gamma\left(\frac{p_0^{q_1} m_0^{q_2} + p_1^{q_1} m_1^{q_2}}{2}\right) + (1-\gamma)\left(p_0^{q_1} m_0^{q_2} + \frac{p_1^{q_1} m_0^{q_2} + p_0^{q_1} m_1^{q_2} + p_1^{q_1} m_1^{q_2}}{4}\right). \tag{17}$$

To avoid distraction, we leave the technical detail leading to (16) in Appendix B. Based on (16), the analytical $f(\alpha_1, \alpha_2)$ can also be found based on the definition (10). Both the analytical τ and f will later be used to compare to the numerical result.

In the numerical experiment, $p_0 = 0.2, p_1 = 0.8$ and $m_0 = 0.4, m_1 = 0.6$ were used to generate the π- and μ-cascades for $g = 1, 0.8, 0.3, 0$. For each g value, 30 sets of π, μ cascades of 16,384 points each were generated. Using the existing WTMM algorithm [2,4], we first locate the maxima lines and estimate the corresponding wavelet modulus maxima for the individual cascade. We then follow (6) to pair up the modulus maxima in (5) to define the joint partition function. As mentioned above, instead of using (8)–(11), the numerical α_1, α_2 and $f(\alpha_1, \alpha_2)$ were estimated by the alternative approach outlined in Appendix A. Finally, $\tau(q_1, q_2)$ is determined by the Legendre transform (9). A set of analyzing wavelets were used in the numerical experiment (below). The first derivative of the Gaussian wavelet appears to give the best result that is reported in this work.

3.2 Numerical results

Typical maxima lines of the coupled cascades are shown in Figure 2. It is observed that the maxima lines are "aligned" when the fractal generation is completely dependent at $g = 1$ and begin to "mis-align" for $g < 1$. The power law scaling of $Z(a; q_1, q_2)$ are found in all cases (Fig. 3).

In Figure 4, the contour of the level set of $f(\alpha_1, \alpha_2)$ are shown on the $\alpha_1 \times \alpha_2$ plane. Superimposed on these figures are the analytical $f(\alpha_1, \alpha_2)$ derived by the Legendre transform of (16). It is evident that the contour lines vary systematically with the g value. When the fractal generating mechanisms are completely dependent of each other ($g = 1$), $f(\alpha_1, \alpha_2)$ describes a one-dimensional curve supported by the functional relationship $\alpha_1(\alpha_2)$. This is expected as any spiking pattern in one cascade automatically implies the same for the other. As a result, the maxima lines will converge at the same location in the time-scale

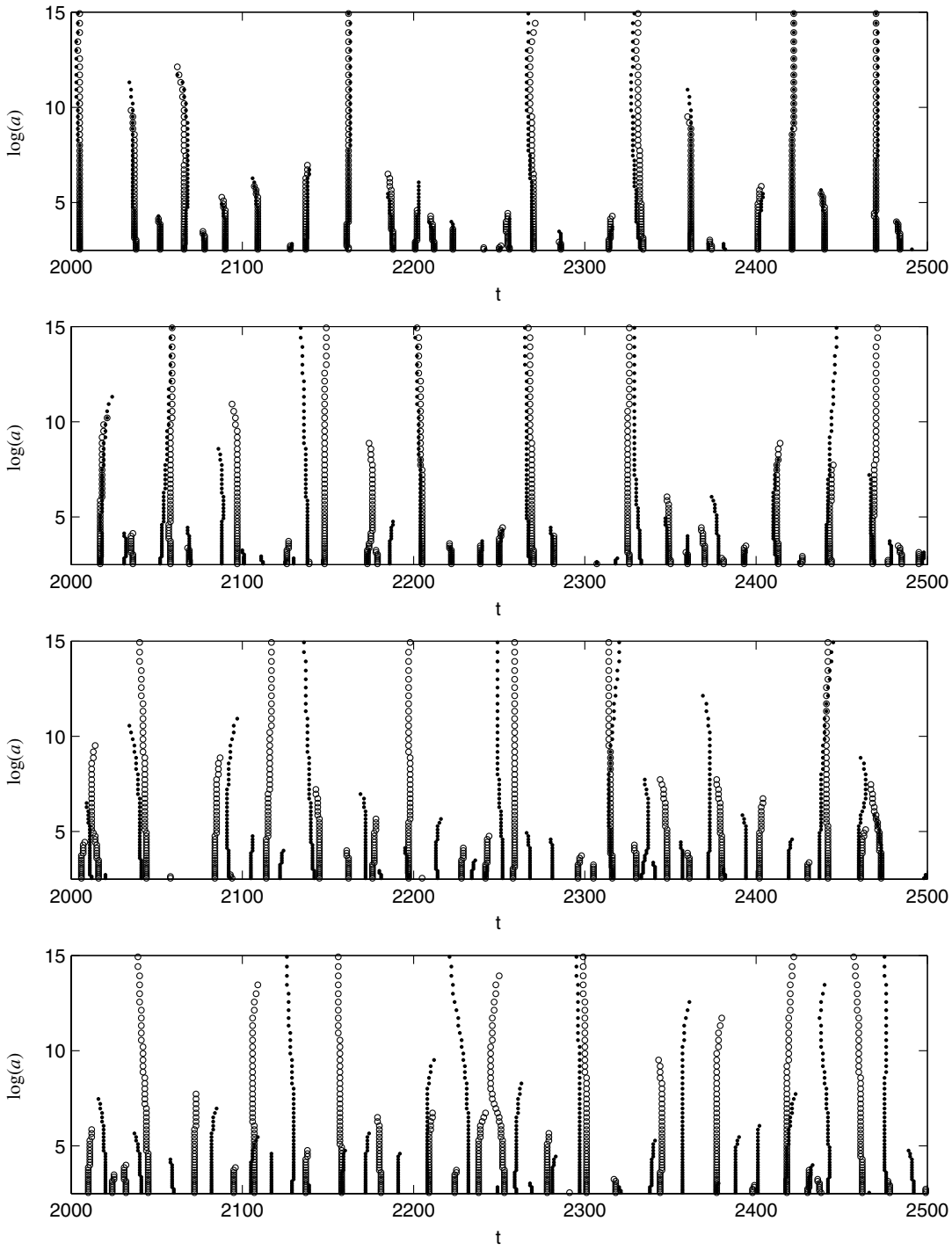

Fig. 2. Typical maxima lines in the time-scale plane from one of the 30 sets of π- ("o") and μ-cascades ("+") with coupling parameter $g = 1.0, 0.8, 0.3, 0.0$ (top to bottom). Notice the perfect alignment of maxima lines for the completely dependent cascades ($g = 1$). First derivative of the Gaussian wavelet is used in the numerical calculation.

plane. This establishes the one-to-one relationship of observing the exponents α_1 and α_2. For $g < 1$, $f(\alpha_1, \alpha_2)$ describes a two-dimensional surface and gives rise to the oval-shape contour lines (Figs. 4b–4d). This means that the observation of α_1 can take place simultaneously for a range of α_2. As a result, the contour line "open up" and cover the largest area when the fractal generations are completely independent from each other at $g = 0$. In addition, the contour lines at $g = 0$ assume a "perfect" orientation that aligns with the $\alpha_1 = 0, \alpha_2 = 0$ axes (Fig. 4d).

Figure 4 shows a good match between the numerical and theoretical $f(\alpha_1, \alpha_2)$. The correlation coefficient ρ (12) can further provide the quantitative difference. The analytical ρ can be obtained by substituting (16) into (12), which yields simply $\rho = g$.

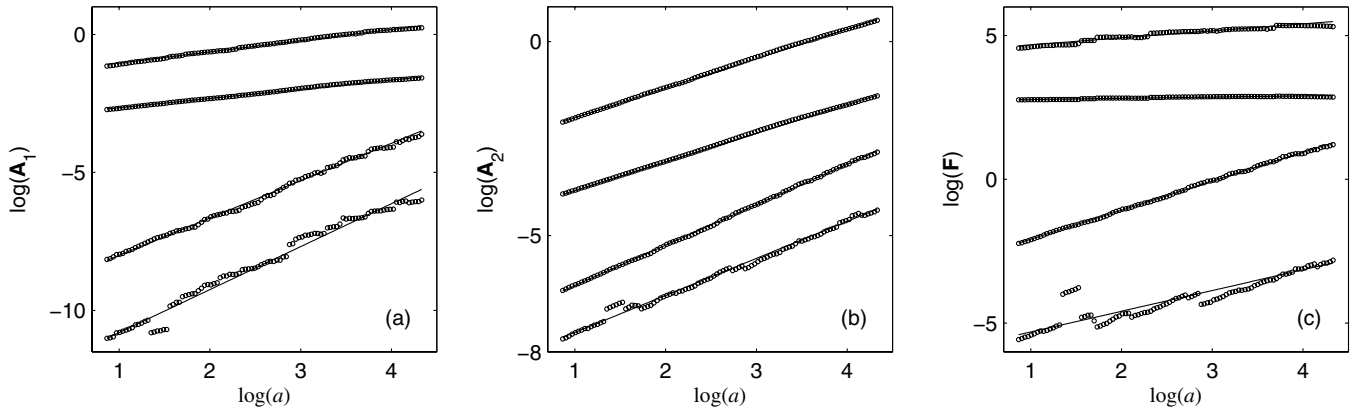

Fig. 3. $\log(\mathbf{A}_1)$, $\log(\mathbf{A}_2)$ and $\log(\mathbf{F})$ vs. $\log(a)$ plots of a typical case of the coupled cascades with $g = 0.8$. The straight lines describes the power laws at $(q_1, q_2) = (3, -2)$, (4,0), (0,0), $(-1, 3)$ (top to bottom). Regression lines are shown as solid lines. The slope of the regression lines are estimated as α_1, α_2 and $f(\alpha_1, \alpha_2)$ based on (14)–(16).

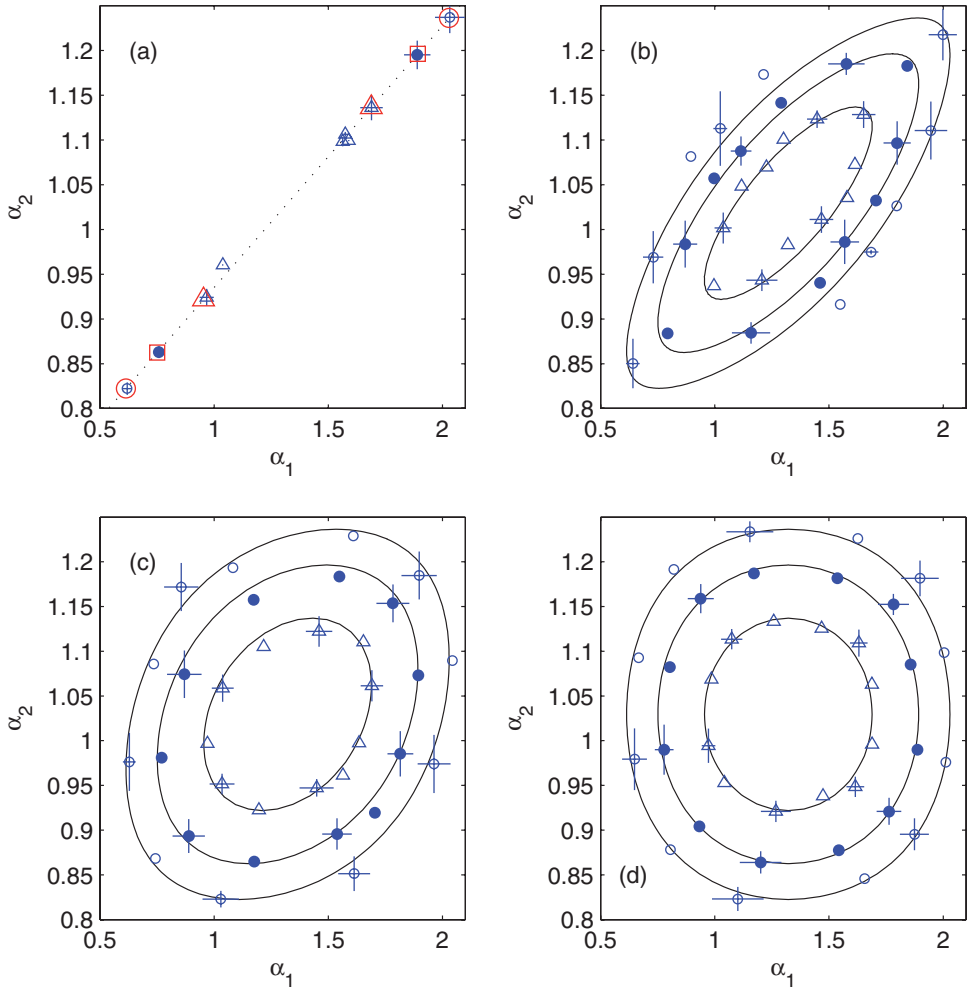

Fig. 4. Averaged contour of the level set of numerical $f(\alpha_1, \alpha_2) = C$ for $C = 0.6$ ("o"), 0.75 ("•"), 0.9 ("△"). Theoretical contour lines are shown as solid lines. The averaging is based on 30 sets of π and μ cascades. Error bars of one standard deviation of selected data points are shown. They are based on the scatter of data points inside a pre-defined uniform grid in the displayed region of the figure. The corresponding g values are (a) 1, (b) 0.8, (c) 0.3, (d) 0. For $g = 1$, $f(\alpha_1, \alpha_2)$ "collapses" into a one-dimensional curve. The projection of the theoretical $f(\alpha_1, \alpha_2)$ is shown as the dotted line. $\{f(\alpha_1, \alpha_2) = C\}$ consists of only two points: $C = 0.9$ ("△"), $C = 0.75$ ("square"), $C = 0.6$, ("o"), are shown (in red).

Table 1. Averaged and analytical ρ values for $g = 0, 0.3, 0.8, 1.0$.

g	0.0	0.3	0.8	1.0
ρ	0.016	0.280	0.775	0.838

The numerical ρ is estimated directly from (12) using the finite difference approximation for the derivatives. Shown in Table 1 are the averaged ρ values based on the 30 sets of π, μ. It is evident that the numerical data matches very well with the analytical result for $g \leq 0.8$. For the completely dependent case ($g = 1$), the discrepancy of $\sim$16% is quite large. This is largely contributed by the finite difference approximation of the small second derivative of $\tau(q_1, q_2)$ at $g = 1$.

In addition to the Gaussian wavelet, the Daubechies family and coiflet family wavelets were also used to compare the result [23]. While the scaling characteristics of $\mathbf{A}_1, \mathbf{A}_2, \mathbf{F}$ are captured in all cases, the degree of accuracy varies. See, for example, the contour of the averaged $\{f(\alpha_1, \alpha_2) = C\}$ obtained by the Haar wavelet (first order Daubechies wavelet) in Figure 5. Using higher order Daubechies or coiflet wavelets does not yield qualitatively different result. In all cases, there is a reasonable agreement in the region of small α_1, α_2. However, discrepancy starts to develop and becomes most pronounced in the area of large α_1, α_2. These Hölder exponents are related to large negative q_1, q_2 values. The loss of accuracy for large negative q_1, q_2 appears to be universal for the two wavelet families we studied. It is interesting to note the sharp contrast with the Gaussian wavelet results (Fig. 4). However, we could not find a satisfactory answer for the superior performance of the Gaussian wavelet in the present application.

Given the numerical data, we also checked the relationship (15) between JPFA and RMA. We first took the numerical $\tau_{\pi/\mu}(q_1)$ to estimate the level set $\tau(q_1, q_2) = 0$. We then applied the so-called deterministic algorithm proposed by Riedi and Scheuring to find $\tau_{\pi/\mu}$. Briefly, the unit interval (0,1) is first divided into smaller intervals $I_k^{(n)}$ of size $2^{(-n)}, n = 1, 2, \cdots$ and then used to define a partition satisfying $\mu \sim \delta$. Finally, $\tau_{\pi/\mu}$ is estimated as the power law exponent in $\sum \pi^q \sim \delta^{\tau_{\pi/\mu}}$; see (14). In Figure 6, the $\tau_{\pi/\mu}(q_1)$ estimated by the two different approaches are shown to match well. Similar match is also found for $\tau_{\mu/\pi}$ (not shown).

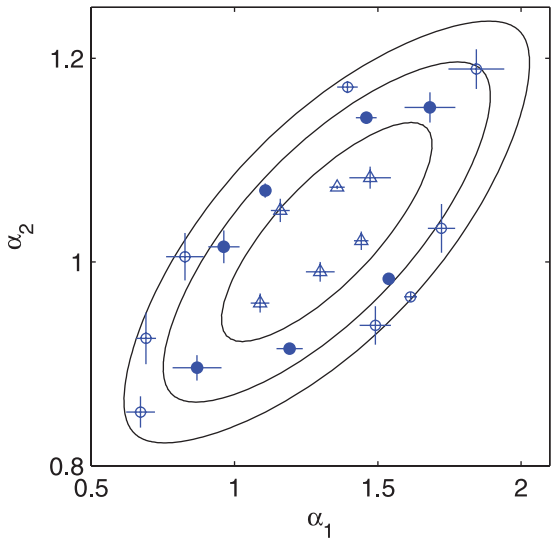

Fig. 5. Averaged contour of the level set of the numerical $f(\alpha_1, \alpha_2) = C$ for $g = 0.8$ and $C = 0.6$ ("o"), 0.75 ("•"), 0.9 ("△"). The result is based on the Haar analyzing wavelet. Theoretical contour lines are shown as solid lines. Error bars of one standard deviation from selected data points are shown. The same case analyzed by the Gaussian wavelet is shown in Figure 4b.

4 Concluding remarks

In this work, a WTMM-based technique is introduced for the first time to estimate the fractal correlation in the framework of the joint partition function analysis proposed by Meneveau et al. [1]. As WTMM has been proven to be one of the most effective tools for singularity analysis [2,3], it is shown that the extension proposed above can also capture accurately the fractal correlation from data fluctuation. We also show that another leading idea, relative multifractal analysis, developed for comparing multifractality, can be considered as a special case of JPFA at a particular parameter setting.

The application using the coupled cascades with various coupling strength shows interesting results. It is encouraging to see that distinctive effect from the coupling of multifractal generating mechanisms does exist and can be captured in $f(\alpha_1, \alpha_2)$ using the WTMM-based JPFA. In particular, the geometry of $f(\alpha_1, \alpha_2)$ changes from a one-dimension object for completely coupled generating mechanisms to a "fully expanded" two-dimensional surface for completely independent generating mechanisms. This trend is at least true for the important class of binomial cascades and is intriguing in its own right. Intuitively, it is possible to have more exotic cases where the fine structure of these manifestations vary. For example, a regular cascade coupled with one that has time-varying weights. However, it is plausible that the general characteristics remain, namely, the stronger the coupling bewteen the multifractal generating mechanisms, the "slenderer" the surface $f(\alpha_1, \alpha_2)$ becomes. This, as well as, applications on different experimental data are the interesting future expansions of this work.

This research is supported by Natural Science and Engineering Research Council of Canada. The authors wish to thank the valuable comments by the anonymous referee.

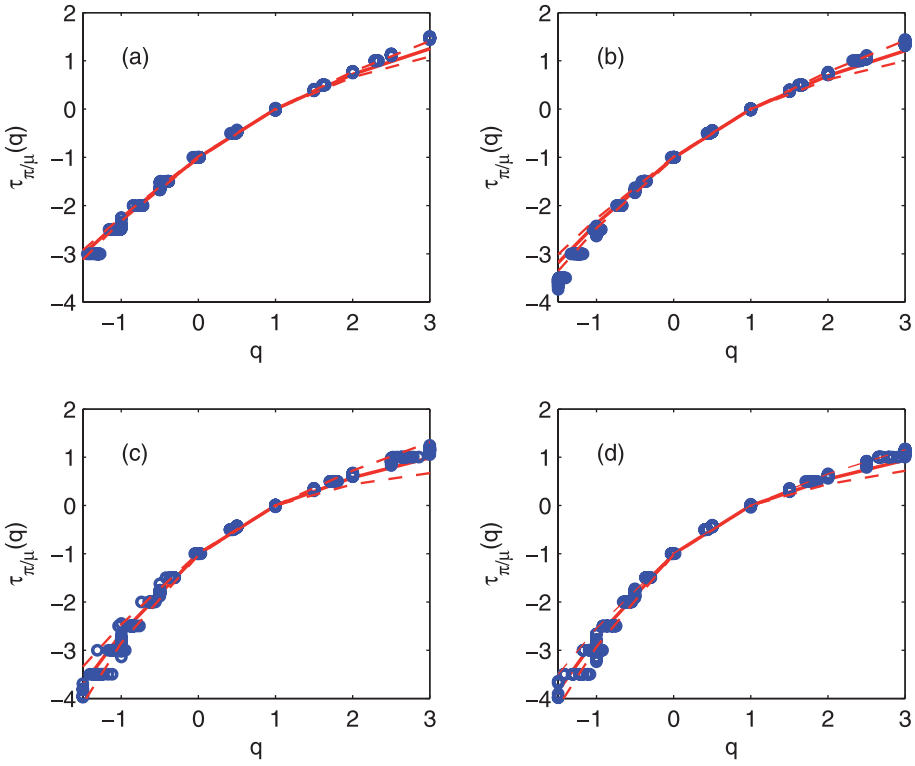

Fig. 6. $\tau_{\pi/\mu}(q)$ estimated by WTMM-based JPFA ("o") method (from the contour line of $\tau(q,p)=0$) and the deterministic algorithm porposed (solid line); see text. The solid lines shown are based on the ensemble average with $\pm$ 3 standard deviation boundaries plotted as long-dashed lines. The g values are (a) 1, (b) 0.8, (c) 0.3, (d) 0.

Appendix A

The Legendre transform (10) relies on using τ estimated from (8). However, there are known factors, such as lacunarity [1, 6, 7], that introduce oscillatory, scale dependent, prefactor. This results in the poor estimate of $\tau(q_1,q_2)$. A remedy to this problem is to introduce

$$\nu(j,a;q_1,q_2)=\frac{C_{1,r(j)}^{q_1}C_{2,s(j)}^{q_2}}{Z(a;q_1,q_2)}. \tag{A.1}$$

Then, by (8) and (10), one has

$$\partial Z(a;q_1,q_2)/\partial q_1 \sim a^{\tau(q_1,q_2)}\log(a)\partial\tau(q_1,q_2)/\partial q_1 = a^{\tau(q_1,q_2)}\log(a)\alpha_1. \tag{A.2}$$

Note the prefactor $\log(a)\alpha_1$ in (A.2) that varies logarithmically with a. From (A.2), one has

$$\sum_j \nu\log(C_{1,j})=\frac{\partial Z/\partial q_1}{Z}. \tag{A.3}$$

Substituting (A.2) into (A.3) yields

$$\mathbf{A}_1(a;q_1,q_2)=\sum_j \nu(j,a;q_1,q_2)\log(C_{1,r(j)})\sim a^{\alpha_1(q_1,q_2)}. \tag{A.4}$$

Note the prefactor in (8) is effectively canceled in (A.4). Similarly, one can show

$$\mathbf{A}_2(a;q_1,q_2)=\sum_j \nu(j,a;q_1,q_2)\log(C_{2,s(j)})\sim a^{\alpha_2(q_1,q_2)}. \tag{A.5}$$

Finally, based on (A.1), one has

$$\sum \nu\log(\nu)=q_1\frac{\partial Z/\partial q_1}{Z}+q_2\frac{\partial Z/\partial q_2}{Z}-\log(Z). \tag{A.6}$$

Substituting (10) and (A.2) into the above results in

$$\mathbf{F}(a;q_1,q_2)= \sum_j \nu(j,a;q_1,q_2)\log(\nu(j,a;q_1,q_2))\sim a^{f(\alpha_1,\alpha_2)}. \tag{A.7}$$

In the numerical experiment, α_1,α_2 and f are estimated from the exponents in (A.4), (A.5) and (A.7).

Appendix B

The derivation of the analytical $\tau(q_1,q_2)$ is based on the coarse grained joint partition function for the coupled cascades:

$$Z_J(a;q_1,q_2)=\sum \pi(I_{r_1,\cdots,r_J})^{q_1}\mu(I_{r_1,\cdots,r_J})^{q_2}.$$

From the combination of γ completely dependent and $(1-\gamma)$ independent proportions, Z_J is found explicitly as

$$Z_J(a;q_1,q_2) \sim (2Y)^J$$

where Y is given by (17). Letting $J \to \infty$, $Z_J \to Z$ and (16) is obtained as the power law exponent of $Z \sim a^{\tau(q_1,q_2)}$.

References

1. C. Meneveau, K.R. Sreenivasan, Phys. Rev. A. **41**, 894 (1990)
2. E. Bacry J.F. Muzy, A. Arneodo, J. Stat. Phys **70**, 635 (1993)
3. S. Jaffard, SIAM J. Math. Anal. **28**, 944 (1997)
4. J.F. Muzy, E. Bacry, A. Arneodo, Phys. Rev. E **47**, 875 (1993); J.F. Muzy, E. Bacry, A. Arneodo, Phys. Rev. Lett. **67**, 3515 (1991); J.F. Muzy, E. Bacry, A. Arneodo, Int. J. Bif. & Chaos **4**, 245 (1994)
5. S. Mallat, W.L. Hwang, IEEE Trans. Info. Theory **38**, 617 (1992)
6. A. Chhabra, R.V. Jensen, Phys. Rev. Lett. **62**, 1327 (1989)
7. C. Meneveau, K.R. Sreenivasan, Phys. Lett. A **137**, 103 (1989)
8. I.R. Cohen, D. Harel, J. Royal Soc. Interf **4**, 175 (2007)
9. T. Di Matteo, Quant. Fin. **7**, 21 (2007)
10. J.O. Fortrat, D. Sigando, R.L. Hughson, A. Maillet, Y. Yamamoto, C. Gharib, Auton. Neurosci. **86**, 192 (2001); also general review in Task Force of the ESC and NASPE, Euro. Heart J. **17**, 354 (1996)
11. J. Lévy-Léhel, R. Riedi, Fractal in Engineering, edited by J. Lévy-Léhel, E. Lutton, C. Tricot (*Springer Verlag*, London, 1997), p. 185
12. Y. Pesin, *Dimension theory in dynamical systems: contemporary views and applications, Chicago Lectures in Mathematics* (Chicago Univ. Press, 1997)
13. J. Lévy-Léhel, R. Vojak, Adv. Appl. Math. **20**, 1 (1998)
14. R.H. Riedi, I. Scheuring, Fractals **5**, 153 (1997)
15. G. Brown, G. Michon, J. Peyrière, J. Stat. Phys **66**, 775 (1992)
16. J. Cole, Chaos, Solitons & Fractals **11**, 2233 (2000)
17. H.G.E. Hentschel, I. Procaccia, Physica D **8**, 435 (1983)
18. M.H. Halsey et al., Phys. Rev. A **33**, 1141 (1986)
19. D. Schertzer, S. Lovejoy, *Space/Time Variability and Interdependencies in Hydrological Processes*, edited by R.A. Feddes (Cambridge Univ. Press, 1995) p. 153
20. A.N. Kravchenko, D.G. Bullock, Agron. J. **92**, 1279 (2000)
21. T.B. Zeleke Takele B. Zeleke, Bing Cheng Si, Soil Sci. Soc. Am. J. **69**, 1691 (2005)
22. W-X. Zhou, D. Sornette, e-print `arXiv:cond-mat/0408600` (2004)
23. I. Daubechies, *Ten Lectures on Wavelets*, CBMS-NSF Lect. Notes, SIAM **61** (1992)